Applied Physics Letters

Direct observation of proximity-induced magnetism and spin reorientation in topological insulator on a ferrimagnetic oxide

Cite as: Appl. Phys. Lett. **114**, 082403 (2019); https://doi.org/10.1063/1.5083931
Submitted: 02 December 2018 . Accepted: 11 February 2019 . Published Online: 28 February 2019

Chao-Yao Yang, Yen-Hsun Lee, Kui-Hon Ou Yang, Kuan-Chia Chiu, Chi Tang, Yawen Liu, Yi-Fan Zhao, Cui-Zu Chang, Fan-Hsiu Chang, Hong-Ji Lin, Jing Shi, and Minn-Tsong Lin

Applied Physics Letters ARTICLE scitation.org/journal/apl

Direct observation of proximity-induced magnetism and spin reorientation in topological insulator on a ferrimagnetic oxide

Cite as: Appl. Phys. Lett. **114**, 082403 (2019); doi: 10.1063/1.5083931
Submitted: 2 December 2018 · Accepted: 11 February 2019 ·
Published Online: 28 February 2019

Chao-Yao Yang,[1] Yen-Hsun Lee,[1] Kui-Hon Ou Yang,[1] Kuan-Chia Chiu,[1] Chi Tang,[2] Yawen Liu,[2] Yi-Fan Zhao,[3] Cui-Zu Chang,[3] Fan-Hsiu Chang,[4] Hong-Ji Lin,[4] Jing Shi,[2] and Minn-Tsong Lin[1,5,6,a)]

AFFILIATIONS

[1]Department of Physics, National Taiwan University, Taipei 10617, Taiwan
[2]Department of Physics and Astronomy, University of California, Riverside, California 92521, USA
[3]Department of Physics, The Pennsylvania State University, University Park, Pennsylvania 16802, USA
[4]National Synchrotron Radiation Research Center, Taiwan, 101 Hsin Ann Road, Hsinchu Science Park, Hsinchu 30076, Taiwan
[5]Institute of Atomic and Molecular Sciences, Academia Sinica, Taipei 10617, Taiwan
[6]Research Center for Applied Sciences, Academia Sinica, Taipei 11529, Taiwan

[a)]**Author to whom correspondence should be addressed:** mtlin@phys.ntu.edu.tw

ABSTRACT

The quantum anomalous Hall effect (QAHE) in a magnetic topological insulator system without the need of an external magnetic field becomes of great interest because of its dissipationless spin currents. The proximity effect via a magnetic adlayer is a promising strategy to bring magnetism into a topological insulator (TI) due to its boosted Curie temperature for a realistic application. In this work, a proximity-induced magnetism above 90 K in a TI, $(Bi_{0.25}Sb_{0.75})_2Te_3$, on a ferrimagnetic adlayer with perpendicular magnetic anisotropy, thulium-iron-garnet (TIG), was evidenced directly by using magnetic circular dichroism. A competition between exchange couplings with different sublattice-sites was further revealed element-specifically in a temperature-driven spin-reorientation of TI, bringing an issue on magnetic inhomogeneity at the interface, which might cause difficulties in obtaining QAHE in such a TI/TIG bilayer system. Our results prove directly the robust magnetism of TI above liquid nitrogen temperatures and also give a deep insight into the mechanism of interfacial coupling in the proximity effect for the bilayer of TI and magnetic oxide, which could be essential for the design of a system with QAHE.

The quantum anomalous Hall effect (QAHE) in topological insulators (TI), arising from the topological band structure under broken time-reversal symmetry, has opened a horizon of quantum physics and emerged as a member of the Hall effect family.[1,2] QAHE serves as a unique playground for dissipationless quantized spin current at the edge and is thus a potential candidate for use in quantum spintronics.[1,2] In order to realize the QAHE, one needs to have a magnetic topological insulator system with perpendicular anisotropy. Such a system was experimentally demonstrated in a magnetically doped TI at an extremely low temperature (~1.5 K),[1] and even the very recent study on the existing magnetism observed at 5 K (Ref. 3) still faces the fundamental challenge of a very low Curie temperature. This limits very much a realistic application of QAHE with the system of magnetic doping into TI.

On the contrary, an effective strategy by using the magnetic proximity effect (MPE) to magnetize the TI has been reported in several TI-based systems,[4–6] which could reach a much higher Curie temperature even up to room temperature, for example, on a bilayer system with TI deposited on a magnetic oxide with perpendicular anisotropy (thulium-iron-garnet, TIG),[6] suggesting a strong exchange interaction in such an MPE heterostructure. However, the proximity effect induced magnetism here has been demonstrated only *indirectly* in a transport measurement of the anomalous Hall effect (AHE),[4,6] whose origin might be as a result of the combined MPE and spin-Hall effect at the interface of a magnetic heterostructure,[7] leading to the ambiguity of interpretation of the measured transport signals. The detailed electronic properties and the coupling mechanism of MPE in TI,

which could be critical for the existence of QAHE, are only poorly understood. Therefore, the direct evidence of magnetism in TI and detailed understanding of magnetic coupling between TI and magnetic oxide *via* the proximity effect are urgently desired. The present work provides direct evidence of the proximity-induced magnetism of TI adjacent to TIG in the application of x-ray magnetic circular dichroism (XMCD), which probes directly to material magnetism. The element specificity of the magnetic probe was able to figure out a kind of temperature-driven spin-reorientation transition of the magnetic moment on the Te's valence 5*p*-orbit of TI. This finding further enlightens a competing mechanism of the exchange couplings of Te with different sub-lattice elements Fe and Tm in TIG, which could be essential for understanding the necessary condition of interfacial magnetism for realizing QAHE in TI.

The stack of NGG_{sub}/TIG(15)/TI(5)/Te(5) was fabricated by the combined pulsed laser deposition (PLD) and molecular beam epitaxial (MBE) technique, and the thickness is in nanometer. The employed TI in this work is $(Bi_{0.25}Sb_{0.75})_2Te_3$ with 5 quintuple layer (QL) in thickness, and the stoichiometry was controlled by the Knudsen effusion cell during MBE co-evaporation. Experimental details for material growth and XMCD measurements are given in the supplementary material. The sharp interface between TI and TIG exhibited by Tang *et al.*[6] ensures the quality of the sample to study MPE.

Figure 1(a) shows the stack of the TI-TIG magneto-heterostructure. The epitaxial lattice structure and the magnetic structure are depicted schematically in Fig. 1(b) with Fe(a) and Fe(d) representing Fe with octahedral coordination and tetrahedral coordination, respectively. Figures 1(c)–1(f) display the XAS and XMCD at the Fe L_3-edge and at the Tm M_5-edge taken at 300 K and 90 K, respectively. The XMCD spectra in Figs. 1(d) and 1(f) suggest that the two elements contribute their magnetic moments at 90 K and are anti-ferromagnetically (AFM) coupled, as indicated by their opposite sign on the XMCD spectra.[8–11] In Figs. 1(g) and 1(h), the AFM relationship between Fe and Tm is further demonstrated by their element-specific hysteresis curves. Fe yields a larger coercive field than Tm at 90 K, as highlighted by the vertical dashed line in Figs. 1(g) and 1(h). The non-identical coercive field of Fe and Tm in the TIG's sublattices reveals the weak coupling between these two elements, which is also reflected by their different degrees of temperature-dependency on the XMCD spectrum. In contrast to Fe [Fig. 1(d)], the XMCD spectra of Tm [Fig. 1(f)] nearly vanishes at 300 K but increases sharply when the temperature is reduced to 90 K, suggesting a remarkable magnetic sensitivity of Tm in response to the temperature. In other words, the ferromagnetism of Tm could be effectively recovered by reducing the temperature.

Figure 2(a) shows the XMCD spectra for further characterization at the Fe L_3-edge at 20 K with field-cooling (FC) and zero field-cooling (ZFC) treatments. Considering the strong perpendicular anisotropy of TIG,[6,12,13] the observed quenching on XMCD (ZFC) at 20 K should be due to the large coercive field of Fe. Because the H_c of TIG monotonically increases upon reducing temperature, as reported by Tang *et al.* in their

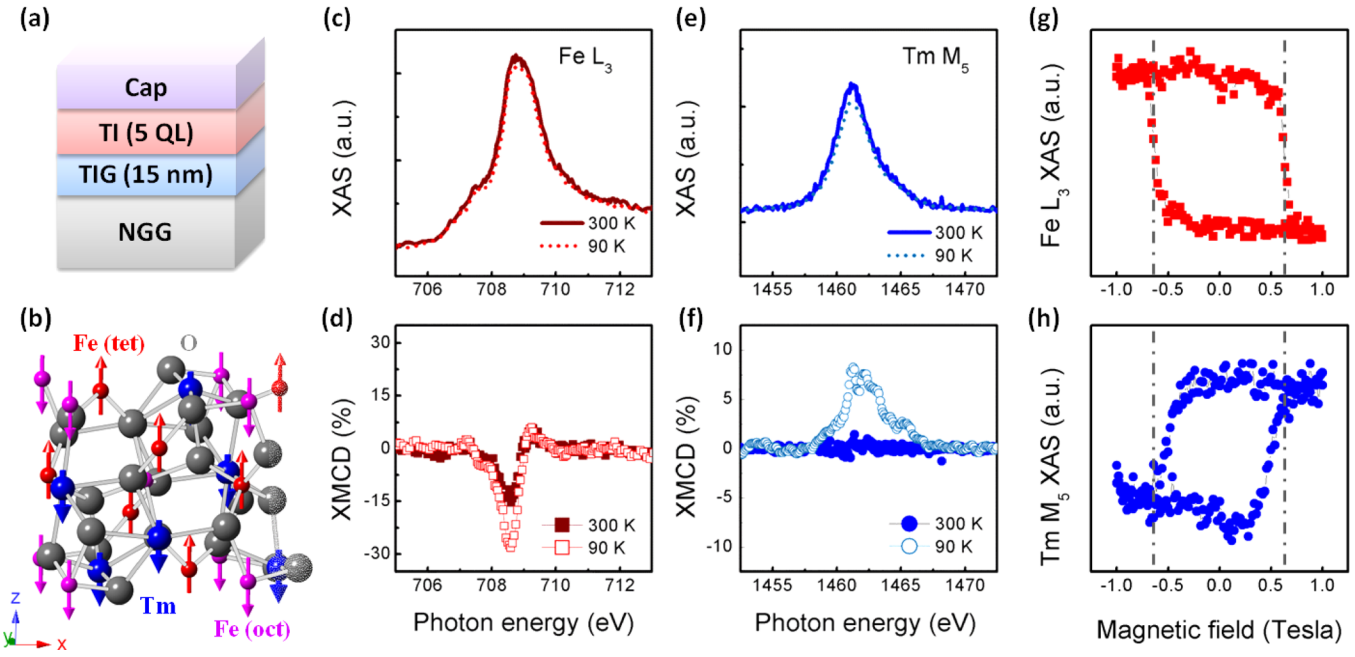

FIG. 1. (a) TI-TIG magneto-heterostructure stack. (b) Epitaxial lattice of the TIG scheme. Fe(a) and Fe(d) represent Fe with octahedral coordination and tetrahedral coordination, respectively. (c) XAS and (d) XMCD asymmetry at the Fe L_3-edge with temperature dependency. (e) XAS and (f) XMCD asymmetry at the Tm M_5-edge with temperature dependency. The element-specific hysteresis curve of (g) Fe and (h) Tm acquired by applying a perpendicular magnetic field with a fixed photon energy at Fe L_3 (708.6 eV) and Tm M_5 (1461.4 eV), respectively, is shown. All spectra were taken by using right-hand circularly polarized x-rays, $\sigma(+)$.

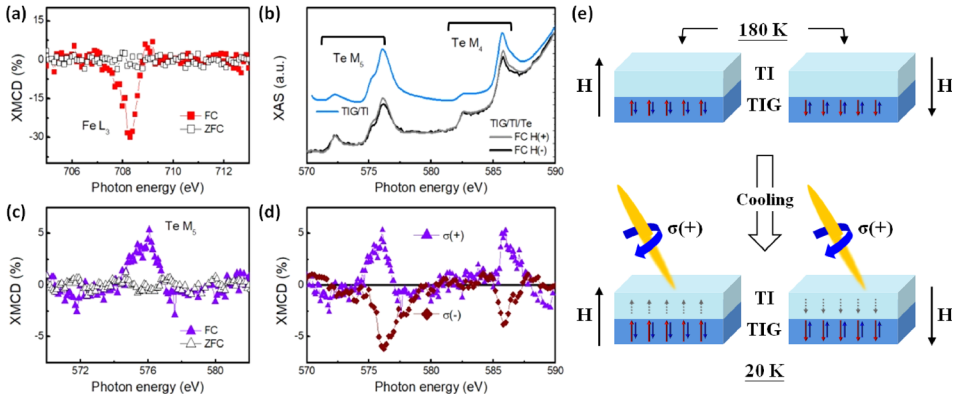

FIG. 2. (a) XMCD asymmetry at the Fe L_3-edge at 20 K obtained after treatment by field-cooling (FC) and zero-field-cooling (ZFC). (b) XAS at Te M_4 and M_5-edges taken at 20 K with two perpendicular FC configurations together with the reference spectrum of TIG/TI (c) XMCD asymmetry at the Te M_5-edge at 20 K obtained after treating FC and ZFC. Spectra in (a)–(c) were acquired by $\sigma(+)$. (d) Te M_4 and M_5-edge XMCD asymmetry at 20 K obtained after treating FC with two opposite x-ray helicities, $\sigma(+)$ and $\sigma(-)$. (e) Schematic diagram to illustrate the FC process and the moment configuration in the TI-TIG magneto-heterostructure at 20 K, referring to the XMCD results in (a) and (c). Arrows in red, blue, and grey represent the magnetic moment of Fe, Tm, and Te, respectively. The magnetization of TIG is dominated by Fe because no magnetic compensation is observed within all the investigated temperatures. The details of the relative coupling among Fe, Tm, and Te are discussed in Fig. 4 and the main text.

supplementary material,[6] H_c at 20 K may be even larger than 1 T in our case (see supplementary material 1). It implies that the limited magnetic field (1 T) cannot drive the magnetization switching of Fe and hence the absence of XMCD. However, it was restored by treating the FC as shown in Fig. 2(a) [see the method section in supplementary material and Fig. 2(e)]. On the other hand, Figs. 2(b) and 2(c) show the XAS at Te $M_{4,5}$ edges and the XMCD at the Te M_5 edge, respectively. To eliminate the contribution from the capping layer, a reference spectrum of the sample without the Te cap is also put together for a comparison. Consequently, following the pattern as Fe, a distinguishable XMCD signal at Te M_5 [Fig. 2(c)] could also be detected using the FC treatment, whereas the XMCD using ZFC is still absent. The result indicates that the magnetic state on the Te's valence orbit should switch with Fe's magnetization reversal. The XMCD at the Te M_5 edge appeared when the XMCD at the Fe L_3 edge was triggered by FC, which serves as an indicator of the MPE-induced magnetism. The XMCD at Fe L_3 and Te M_5 edges features opposite signs, pointing down for Fe L_3 and pointing up for Te M_5. This reveals the FM coupled nature between these two elements defined by the inverse electronic transition symmetry,[14–16] which is discussed in the following paragraph. Figure 2(d) presents the full range XMCD survey across the Te M_4 and M_5 edges using $\sigma(+)$ along with the result by $\sigma(-)$. As shown in Fig. 2(d), the antisymmetric XMCD spectra acquired by $\sigma(+)$ and $\sigma(-)$ confirm the magnetic polarization on the Te's unoccupied state above the Fermi-level. For a better understanding of the XMCD results of Fe and Te using the experimental procedure, Fig. 2(e) illustrates the FC process and the corresponding moment configuration of the TI-TIG magneto-heterostructure, referring to their XMCD sign taken with FC at 20 K. Note that the same sign on Te $M_{4,5}$ XMCD is non-typical and also observed in other related studies[17–19] which would not be discussed in detail in this work.

Figure 3(a) shows an extended XMCD characterization at the Te M_5 edge at 90 K (without FC) and superimposes the result over the spectra of Fig. 2(d) (with FC) to monitor the temperature dependency. Both XMCD intensities at Te M_5 (576.1 eV) acquired by $\sigma(+)$ and $\sigma(-)$ reduce significantly at 90 K and vanish at 180 K, suggesting that the detectable Curie temperature of the induced magnetism exceeds 90 K. Another essential discovery is an XMCD sign inversion when the temperature increases from 20 K to 90 K. Figure 3(b) plots the Te M_5 (576.1 eV) XMCD intensity acquired by $\sigma(+)$ and $\sigma(-)$ as a function of the temperature. Again, the symmetric $\sigma(+)$ and $\sigma(-)$ XMCD varying with temperature reflects the magnetic polarization of Te, and the crossover of $\sigma(+)$-$\sigma(-)$ between 20 K and 90 K reveals that a Te spin re-orientation occurs at different temperatures. Because no reversed XMCD was observed on Fe and Tm at all investigated temperatures, the spin re-orientation of Te should not be attributed to the possible compensation effect of TIG due to the lack of XMCD sign inversion on both Fe and Tm.[20–23] Therefore, let us reconsider the effect arising from TIG's sublattices. In Figs. 1(d) and 1(f), the opposite sign of XMCD at the Fe L_3 and Tm M_5 edges reveals the AFM between Fe 3*d* and Tm 4*f* spins to form the ferrimagnetic nature of TIG. In Fig. 2(c), the observed

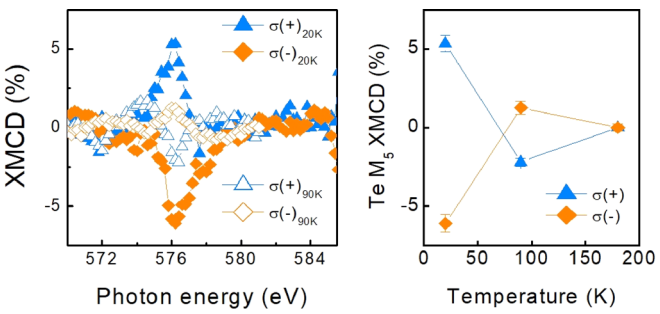

FIG. 3. (a) Temperature-dependent XMCD asymmetry at the Te M_5-edge acquired by $\sigma(+)$ and $\sigma(-)$. (b) Plots of the Te M_5-edge XMCD intensity (at 576.1 eV in (a)) versus temperature.

XMCD at the Te M_5 edge represents a magnetic moment on the Te's valence orbit[14,15] resulting from the interfacial orbital hybridization with Fe 3*d* or Tm 4*f* after introducing an adjacent TIG. Consequently, the opposite sign of XMCD at the Fe L_3 and Te M_5 edges at 20 K reveals that the magnetic moment on the Te 5*p*-orbit is FM coupled with Fe 3*d*[14,15] referring to their inverse electronic transition symmetry, $2p \rightarrow 3d$ for Fe L_3 and $3d \rightarrow 5p$ for Te M_5.[14,15] Hence, Tm 4*f* and Te 5*p* are AFM coupled. Upon increasing the temperature to 90 K, a magnetic phase inversion of Te takes place with reversing Te M_5 XMCD [Fig. 3(b)], whereas the XMCD at the Fe L_3 and Tm M_5 edges is still non-reversed. This indicates that a modification of the Te's magnetic structure is intrinsically triggered by the MPE of TIG while varying the temperature.

Based on the different evolutions on Fe and Tm in response to temperature, we consider the competing relationship between Fe and Tm in contributing to the MPE to Te with a favorable AFM coupling, as reported in other MPE-correlated research systems.[24–26] Figures 1(g) and 1(h) show that Fe and Tm are weakly coupled in the TIG's sub-lattices, which appear on the non-simultaneous magnetization switching at 90 K. This result should be due to the magnetic moment of Tm being mainly from the localized 4*f* band, leading to a weak interaction with neighboring spin, thus yielding a smaller magnetic hardness than Fe and resulting in a limited MPE to the neighboring TI due to the weak Tm 4*f*-Te 5*p* interaction. However, the restored magnetic moment of Tm on the sharp increasing XMCD below 90 K [Fig. 1(f)] suggests that Tm's magnetism would become much more significant as the temperature is further reduced. Once the Tm 4*f*-Te 5*p* interaction can be activated by suppressing thermal fluctuation, Tm plays a significant role in mediating the MPE. It may be attributed to its spatial majority in TIG compared to Fe after considering the compensated Fe in sub-lattices.[19,20] Referring to our analyses of the Fe XMCD fine structure, we also found a magnetic fluctuation of Fe on the tetrahedral site at 20 K, whose moment governs the magnetization of TIG (see supplementary material 2). Under this scope of the inverse competing evolution between Fe and Tm, it is plausible that the exchange coupling would be dominated by the AFM coupled Tm 4*f*-Te 5*p* at low temperatures (20 K) and by Fe 3*d*-Te 5*p* at high temperatures (90 K). The spin re-orientation on Te occurs during the competing evolution between Fe and Tm.

Figure 4(a) plots the correlation of XMCD intensity for all investigated elements versus temperature. Fe clearly plays a dominant role in the evolution of temperature dependency above 90 K due to its sustainable magnetic moment, which remains nearly constant from 90 K to 20 K. On the other hand, Tm should have a more dominating effect on the exchange coupling below 90 K due to its sharp enhancement of the magnetic moment. The absence of the compensation effect in TIG might suggest that the reversed signal of Te XMCD can be explained with the nature that Tm has a dominant effect on the MPE at low temperatures and Fe at higher temperature; otherwise, the monotonic increase in Te's XMCD should be observed rather than the re-orientation. Figure 4(b) illustrates further the picture of the evolution of the exchange coupling among Te, Fe, and

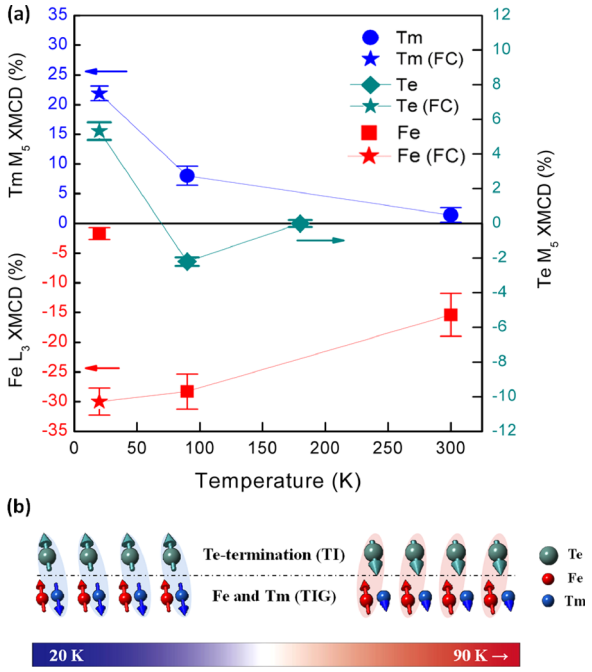

FIG. 4. (a) Plots of the XMCD intensity recorded at Fe L_3 (at 708.6 eV), Tm M_5 (1461.4 eV), and Te M_5 (576.1 eV) edges as a function of temperature. All the XMCD spectra were acquired by $\sigma(+)$ and treated by FC at 20 K, as labeled by stars. (b) Scheme illustrating the exchange coupling between Fe 3*d*, Tm 4*f*, and Te 5*p* moments below and above the magnetic phase inversion temperature.

Tm, based on the observed sign and magnitude of XMCD. At 20 K, the orientation of the magnetic moment of Te was determined by the AFM coupling with Tm 4*f*, while upon increasing the temperature to 90 K, the magnetic moment of the Te is re-orientated as AFM coupling with Fe 3*d* becomes dominant rather than with Tm 4*f*. The spin reversal of Te arises thus from a competing mechanism of AFM exchange coupling of Te with Fe and Tm, respectively, where the MPE was dominated by Tm at 20 K and by Fe at 90 K.

This is an important signature for the operation of the TI-TIG bilayer structure. Based on the XMCD results, we found that the MPE-induced ferromagnetism in TI may suffer from the issue of magnetic homogeneity due to the competing correlation between elements in TIG's sub-lattices. The favorable AFM coupling led by Fe 3*d* (Tm 4*f*)-Te 5*p* competition may not enable a long-range planar exchange at the interface, leading to the sub-domain in TI[3] which is less capable of quantizing the anomalous Hall state on the transport property. This study approached by XMCD provides an element-specific comprehension with respect to the MPE driven by a magnetic compound. The sub-lattice issue should be thus seriously considered.

In conclusion, an element-specific approach with XMCD was used to study the MPE in a TI-TIG magneto-heterostructure with respect to the induced magnetism of the TI and its exchange coupling with an adjacent ferrimagnet. Two major findings have been concluded. First, the proximity-induced

magnetism in a TI compound, $(Bi_{0.25}Sb_{0.75})_2Te_3$, on a perpendicularly magnetic oxide layer was directly evidenced at elevated temperature as compared to the case of magnetic doping.[3] Second, a spin reversal of induced magnetism in TI has been revealed at varying temperatures, indicating a MPE with the competition between exchange couplings of Te with Fe and Tm. This finding does not only help to unveil the origin of exchange coupling in this proximity bilayer but also provides electronic information in MPE, inspiring the critical correlation between the nanomagnetism and transport behavior for the interest of a quantum spintronic system.

See supplementary material for a detailed description for the material growth and XMCD measurement and for element-specific M-H curves of Fe taken at the L_3-edge and normalized XAS and XMCD spectra at the Fe L_3 edge taken at various temperatures.

This work was supported by the Ministry of Science and Technology (MoST) of Taiwan, under Grant No. 105-2119-M-002-013 and as part of the SHINES (Spins and Heat in Nanoscale Electronic Systems), an Energy Frontier Research Center funded by the U.S. Department of Energy, Office of Science, Basic Energy Sciences under Award No. SC0012670. C.Z.C. acknowledges the support from Alan P. Sloan Research Fellowship.

REFERENCES

[1]C.-Z. Chang, J. Zhang, X. Feng, J. Shen, Z. Zhang, M. Guo, K. Li, Y. Ou, P. Wei, L.-L. Wang, Z.-Q. Ji, Y. Feng, S. Ji, X. Chen, J. Jia, X. Dai, Z. Fang, S.-C. Zhang, K. He, Y. Wang, L. Lu, X.-C. Ma, and Q.-K. Xue, Science **340**, 167 (2013).
[2]C.-Z. Chang and M. Li, J. Phys.: Condens. Matter **28**, 123002 (2016).
[3]W. Wang, Y. Ou, C. Liu, Y. Wang, K. He, Q.-K. Xue, and W. Wu, Nat. Phys. **14**, 791 (2018).
[4]Z. Jiang, C.-Z. Chang, C. Tang, P. Wei, J. S. Moodera, and J. Shi, Nano Lett. **15**, 5835 (2015).
[5]M. Lang, M. Montazeri, M. C. Onbasli, X. Kou, Y. Fan, P. Upadhyaya, K. Yao, F. Liu, Y. Jiang, W. Jiang, K. L. Wong, G. Yu, J. Tang, T. Nie, L. He, R. N. Schwartz, Y. Wang, C. A. Ross, and K. L. Wang, Nano Lett. **14**, 3459 (2014).
[6]C. Tang, C.-Z. Chang, G. Zhao, Y. Liu, Z. Jiang, C.-X. Liu, M. R. McCartney, D. J. Smith, T. Chen, J. S. Moodera, and J. Shi, Sci. Adv. **3**, e1700307 (2017).
[7]Q. Shao, A. Grutter, Y. Liu, G. Yu, C. Y. Yang, D. A. Gilbert, E. Arenholz, P. Shafer, X. Che, C. Tang, M. Aldosary, A. Navabi, Q. L. He, B. J. Kirby, J. Shi, and K. L. Wang, preprint arXiv:1811.08574 (2018).
[8]V. López-Flores, N. Bergeard, V. Halté, C. Stamm, N. Pontius, M. Hehn, E. Otero, E. Beaurepaire, and C. Boeglin, Phys. Rev. B **87**, 214412 (2013).
[9]K. Chen, D. Lott, F. Radu, F. Choueikani, E. Otero, and P. Ohresser, Sci. Rep. **5**, 18377 (2015).
[10]A. I. Figueroa, A. A. Baker, S. E. Harrison, K. Kummer, G. van der Laan, and T. Hesjedal, J. Magn. Magn. Mater. **422**, 93 (2017).
[11]W. Zhang, D. Zhang, P. K. J. Wong, H. Yuan, S. Jiang, G. van der Laan, Y. Zhai, and Z. Lu, ACS Appl. Mater. Interfaces **7**, 17070 (2015).
[12]M. Kubota, A. Tsukazaki, F. Kagawa, K. Shibuya, Y. Tokunaga, M. Kawasaki, and Y. Tokura, Appl. Phys. Exp. **5**, 103002 (2012).
[13]C. Tang, P. Sellappan, Y. Liu, Y. Xu, J. E. Garay, and J. Shi, Phys. Rev. B **94**, 140403(R) (2016).
[14]M. Ye, W. Li, S. Zhu, Y. Takeda, Y. Saitoh, J. Wang, H. Pan, M. Nurmamat, K. Sumida, F. Ji, Z. Liu, H. Yang, Z. Liu, D. Shen, A. Kimura, S. Qiao, and X. Xie, Nat. Commun. **6**, 8913 (2015).
[15]L. B. Duffy, A. I. Figueroa, Ł. Gładczuk, N.-J. Steinke, K. Kummer, G. van der Laan, G. van der Laan, and T. Hesjedal, Phys. Rev. B **95**, 224422 (2017).
[16]A. Kimura, S. Suga, T. Shishidou, S. Imada, T. Muro, S. Y. Park, T. Miyahara, T. Kaneko, and T. Kanomata, Phys. Rev. B **56**, 6021 (1997).
[17]F. Wilhelm, R. Eloirdi, J. Rusz, R. Springell, E. Colineau, J.-C. Griveau, P. M. Oppeneer, R. Caciuffo, A. Rogalev, and G. H. Lander, Phys. Rev. B **88**, 024424 (2013).
[18]J. Goulon, A. Rogalev, G. Goujon, F. Wilhelm, J. B. Youssef, C. Gros, J.-M. Barbe, and R. Guilard, Int. J. Mol. Sci. **12**, 8797 (2011).
[19]A. Quindeau, C. O. Avci, W. Liu, C. Sun, M. Mann, A. S. Tang, M. C. Onbasli, D. Bono, P. M. Voyles, Y. Xu, J. Robinson, G. S. D. Beach, and C. A. Ross, Adv. Electron. Mater. **3**, 1600376 (2017).
[20]H. Maruyama and N. Kawamura, J. Electron Spectrosc. Relat. Phenom. **136**, 135 (2004).
[21]J. S. McCloy and B. Walsh, IEEE Trans. Magn. **49**, 4253 (2013).
[22]M. S. Lataifeh and A. Al-sharif, Appl. Phys. A **61**, 415 (1995).
[23]S. Geller, J. P. Remeika, R. C. Sherwood, H. J. Williams, and G. P. Espinosa, Phys. Rev. **137**, A1034 (1965).
[24]H. Wende, Rep. Prog. Phys. **67**, 2105 (2004).
[25]S. M. Suturin, V. V. Fedorov, A. G. Banshchikov, D. A. Baranov, K. V. Koshmak, P. Torelli, J. Fujii, G. Panaccione, K. Amemiya, M. Sakamaki, T. Nakamura, M. Tabuchi, L. Pasquali, and N. S. Sokolov, J. Phys.: Condens. Matter **25**, 046002 (2013).
[26]F. Maccherozzi, M. Sperl, G. Panaccione, J. Minár, S. Polesya, H. Ebert, U. Wurstbauer, M. Hochstrasser, G. Rossi, G. Woltersdorf, W. Wegscheider, and C. H. Back, Phys. Rev. Lett. **101**, 267201 (2008).